First-Principles Simulations of C−S Bond Cleavage in Rhenium Thioether Complexes

Alessandra Magistrato,*,†,§ Patrick Maurer,† Thomas Fässler,‡ and Ursula Rothlisberger,†,||

Laboratory of Inorganic Chemistry, ETH Hoenggerberg, CH-8093, Zürich, Switzerland, and Eduard Zintl Insitute, D-64289 Darmstadt, Germany

Received: December 19, 2003

We present first-principles molecular dynamics studies of the reductive C−S bond cleavage reaction in hexathioether complexes of the form $[Re(9S3)_2]^{m+}$ (with 9S3 = 1,4,7 trithiacyclononane and $m = 1,2$). Our calculations show that electron transfer and bond dissociation take place as two distinct consecutive reaction steps. For the reduced complex, C−S bond fission and subsequent release of ethene can be observed directly at only slightly elevated temperatures. Car-Parrinello molecular dynamics of the reactive process demonstrate that for the dissociation to occur two carbon−sulfur bonds have to be broken quasi simultaneously. For the oxidized form on the other hand, no release of ethene takes place at the same temperature within the limited time scale of our simulations. The activation energies of the dissociation process calculated at the gradient-corrected density functional (BP) level are 21 and 10 kcal/mol for the oxidized and the reduced form, respectively. A detailed analysis of the electronic structure in the transition states confirms the presence of a strong π-back-donation from rhenium d-orbitals into antibonding σ*-orbitals of the C−S bonds that is responsible for the pronounced weakening of the carbon−sulfur bond upon reduction.

1. Introduction

Metal complexes with radioactive nuclei find multiple applications in medicine as tumor, organ, and tissue imaging agents.[1,2] Radioisotopes such as the β-emitting ^{186}Re and ^{188}Re have also found recent use for the in-situ treatment of cancerous tissues.[3,4] A central issue in the development of radiopharmaceuticals with improved imaging and therapeutic properties is the search for compounds with enhanced selectivity. Unfortunately, a rational design of highly selective agents is hampered by the limited knowledge of the factors determining their biodistribution and their targeting abilities on the molecular level. In practice, upon injection in the human body, these molecules encounter a variety of different chemical environments and their pathways and final destinations are crucially determined by their chemical transformations under these varying external conditions. A characterization of the detailed physicochemical behavior of these compounds is therefore important to assist the efforts in the development of new radiopharmaceuticals with improved features.

Rhenium complexes of the form $[Re(9S3)_2]^{m+}$ are potential radiopharmaceutical agents, and a detailed understanding of their properties is thus of direct practical interest. Moreover, these compounds exhibit also interesting chemical characteristics. In the presence of reducing agents such as ascorbic acid, Zn, Cr, or $SnCl_2$, they undergo instantaneous C−S bond cleavage to yield ethene and $[Re(9S3)L]^+$ (where $L = SCH_2CH_2SCH_2CH_2S$) (Figure 1).[5] This cleavage occurs under mild conditions, in aqueous solution, and at room temperature. Experimental and semiempirical calculations at the Extended Huckel level[6] suggest a possible π-back-donation from donor t_{2g}-metal-orbitals into antibonding C−S σ*-orbitals of the thioether ligands as possible cause for the occurrence of reductive bond fission.

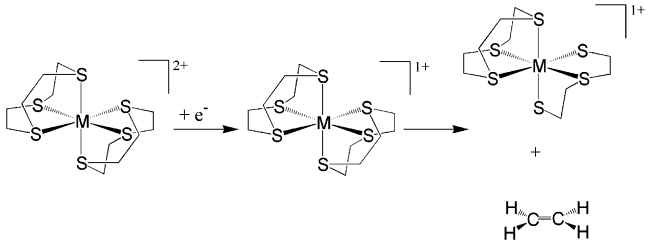

Figure 1. Schematic representation of the reductive C−S bond cleavage in $[Re(9S3)_2]^{2+}$. The reaction occurs at room temperature, in aqueous solution and in the presence of reducing agents such as ascorbic acid, Zn, Cr, and $SnCl_2$.[5a]

The ease in which the C−S bond cleavage can be induced suggests that these simple systems could also serve as homogeneous model compounds for the complex processes involved in the industrial hydrodesulfurization (HDS) of crude oils.[7] HDS requires the use of heterogeneous catalysts, which contain molybdenum and other transition metals oxides and sulfides. The great practical importance of this reaction has stimulated many coordination studies of thiophene to transition metal compounds designed with the goal of activating C−S bonds for cleavage.[8]

In this article, we present a detailed characterization of the structural, electronic, and dynamic properties of rhenium thioether compounds with first-principles molecular dynamics simulations. Our study provides a detailed understanding of the mechanism of the reductive C−S bond cleavage in these systems and thus contributes to a comprehensive characterization of the chemical behavior of these radioactive agents in redox active environments.

* Author to whom correspondence should be addressed. E-mail: alema@sissa.it.

† Laboratory of Inorganic Chemistry, ETH Zentrum.

‡ Eduard Zintl Insitute.

§ Current Address: INFM-Democritos Center and International School of Advanced Studies (SISSA/ISAS), Via Beirut 2-4, I-34014 Trieste, Italy.

|| Current Address: Institute of Molecular and Biological Chemistry, Federal Institute of Technology (EPFL), CH-1015, Lausanne, Switzerland.

10.1021/jp037932k CCC: $27.50
Published on Web 02/11/2004

2. Details of the Computational Scheme

The method of first-principles molecular dynamics simulations, as introduced by Car and Parrinello,[9] has been reviewed in a number of publications.[10]

These simulations combine a classical molecular dynamics (MD) scheme with an electronic structure calculation in the framework of density functional theory (DFT), a pseudopotential formalism, periodic boundary conditions and a basis set of plane waves. All the calculations presented here were performed with the program CPMD.[11] In this study, we used an analytical local pseudopotential for hydrogen and nonlocal, normconserving pseudopotentials of the Martins-Trouiller type[12] for all the other elements. Angular momentum components up to $l_{max} = 1$ and $l_{max} = 2$ have been included for carbon and sulfur, respectively. For rhenium we have constructed a semicore pseudopotential with an ionic reference state of $5s^25p^65d^66s^0$ and cutoff radii of $r_s = 1.1$ au, $r_p = 1.2$ au, and $r_d = 1.45$ au. The 16 valence electrons ($4s^24p^65s^25d^66s^0$) have been treated explicitly, and the pseudopotential also incorporates scalar relativistic effects.

All pseudopotentials have been transformed to a fully nonlocal form using the scheme developed by Kleinman and Bylander,[13] with the exception of rhenium where the nonlocal part of the pseudopotential has been integrated numerically using a Gauss-Hermite quadrature. A point of central importance for the performance of our computational scheme is the quality of the pseudopotential for the transition metal atom. A probe of its accuracy is provided by test calculations performed on ReF_6 and by the calculation of the ionization potentials of rhenium atom (see Supporting Information).

All subsequent calculations were performed with two different popular descriptions for the exchange-correlation functional. In both cases, the exchange part was described with the gradient-corrected model developed by Becke(B),[14] whereas the correlation part was either treated with the formulation due to Perdew (P)[15] or the one due to Lee, Yang, and Parr (LYP).[16] The resulting DFT models, BP and BLYP, respectively, differ solely in the description of the correlation energy. Thus, a comparison of the results obtained by these two functionals provides a direct indication of the importance of correlation effects. A kinetic energy cutoff of 70 Ry was used for all the calculations.

To treat the charged complexes, periodic images were decoupled using the scheme of Hockney.[17] In initial calculations, a simple cubic (SC) cell of edge $a = 21$ au was used, whereas final results are given for a SC cell of edge $a = 25$ au. Molecular dynamics runs at elevated temperatures were performed in the larger SC cell of $a = 25$ au.

For the first-principles molecular dynamics runs, the classical equations of motion were integrated with a velocity Verlet algorithm with a time step of 0.145 fs and a fictitious mass for the electronic degrees of freedom of $\mu = 400$ au. All the calculations were performed within a spin unrestricted formalism.

3. Results and Discussion

3.1. Structural and Electronic Properties of Oxidized and Reduced Compounds. As a first step, we have characterized the structural properties of the rhenium thioether complexes in the reactant ($[Re(9S3)_2]^{2+}$) and in the product ($[Re(9S3)L]^+$, where $L = SCH_2CH_2SCH_2CH_2S$) states.

The starting point of our calculations was the crystal structure of the $[Re(9S3)_2]^{2+}$ complex.[18] The excellent agreement between the X-ray structure and the fully optimized gas-phase geometry[18,19] is shown in Figure 2, as a superposition of experimental and calculated structures, and in Table 1, comparing characteristic structural parameters. Consistent with other studies on transition metal complexes,[20,21] the BP functional leads to slightly better results. All bond lengths are reproduced within $\Delta d \leq 0.03$ Å (2% relative error) with the BP functional, whereas we find a slightly higher deviation of $\Delta d \leq 0.05$ Å (3% relative error) with BLYP.

We have also performed a structural analysis of the dissociation product $[Re(9S3)L]^+$ ($L = SCH_2CH_2SCH_2CH_2S$) using the two different exchange-correlation functionals (Table 2). The observed deviations with respect to the experimental structures

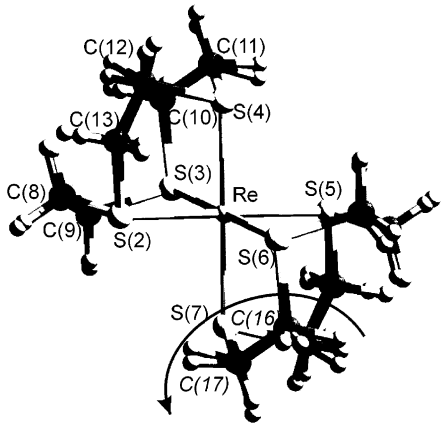

Figure 2. Superposition of the X-ray[18] and the calculated structure (BP functional) for the $[Re(9S3)_2]^{2+}$ compound. The departing ethene molecule is indicated with an arrow.

TABLE 1: Comparison of Crystallographic (exp)[18] and Calculated (BP and BLYP functionals) Bond Lengths (Å) for $[Re(9S3)_2]^{2+}$ and $[Re(9S3)_2]^+$ [a]

	$[Re(9S3)_2]^{2+}$			$[Re(9S3)_2]^+$	
bond	exp	BLYP	BP	BLYP	BP
Re−S(2)	2.38	2.41	2.38	2.39	2.36
Re−S(3)	2.37	2.41	2.37	2.39	2.36
Re−S(4)	2.37	2.41	2.38	2.39	2.35
S(2)−C(8)	1.84	1.89	1.87	1.92	1.89
S(2)−C(13)	1.83	1.86	1.85	1.88	1.86
S(3)−C(9)	1.81	1.87	1.85	1.88	1.86
S(3)−C(10)	1.81	1.89	1.87	1.91	1.89
S(4)−C(11)	1.85	1.87	1.85	1.88	1.86
S(4)−C(12)	1.81	1.89	1.87	1.91	1.89
C(8)−C(9)	1.51	1.53	1.52	1.52	1.52

[a] The atomic labeling scheme is given in Figure 2.

TABLE 2: Comparison of Crystallographic (exp)[5a] and Calculated (BP and BLYP functionals) Bond Lengths (Å) for $[Re(9S3)L]^{2+}$ and $[Re(9S3)L]^+$ ($L = SCH_2CH_2SCH_2CH_2S$) Complexes[a]

	$[Re(9S3)L]^{2+}$		$[Re(9S3)L]^+$		
bond	BLYP	BP	(exp)	BLYP	BP
Re−S(2)	2.41	2.38	2.39	2.42	2.38
Re−S(3)	2.54	2.49	2.44	2.58	2.53
Re−S(4)	2.50	2.49	2.46	2.60	2.54
Re−S(5)	2.39	2.37	2.35	2.40	2.36
Re−S(6)	2.28	2.26	2.26	2.28	2.25
Re−S(7)	2.27	2.26	2.27	2.27	2.26
S(2)−C(8)	1.90	1.88	1.83	1.88	1.86
S(2)−C(13)	1.88	1.85	1.85	1.86	1.83
S(3)−C(9)	1.87	1.85	1.83	1.86	1.84
S(3)−C(10)	1.86	1.84	1.82	1.86	1.84
S(4)−C(11)	1.85	1.83	1.82	1.85	1.83
S(4)−C(12)	1.89	1.87	1.82	1.87	1.86
C(8)−C(9)	1.52	1.52	1.52	1.53	1.52

[a] The atomic labeling scheme is given in Figure 2.

TABLE 3: Calculated Bond Orders[22] for Selected Bonds[a]

bond	$[Re(9S3)_2]^{2+}$	$[Re(9S3)_2]^{+}$	$[Re(9S3)_2]^{2+}$ TS	$[Re(9S3)_2]^{+}$ TS	$[Re(9S3)L]^{2+}$	$[Re(9S3)L]^{+}$
Re−S(6)	0.41	0.44	0.77	0.82	0.87	0.83
Re−S(7)	0.41	0.44	0.77	0.83	0.86	0.83
S(2)−C(8)	0.85	0.82	0.87	0.85	0.87	0.85
S(3)−C(9)	0.88	0.85	0.92	0.89	0.92	0.88
S(6)−C(16)	0.85	0.82	0.22	0.04		
S(7)−C(17)	0.88	0.85	0.23	0.04		
C(8)−C(9)	1.00	1.01	0.99	1.00	0.99	1.00
C(16)−C(17)	1.00	1.01	1.61	1.90		

[a] The atomic labeling scheme is given in Figure 2.

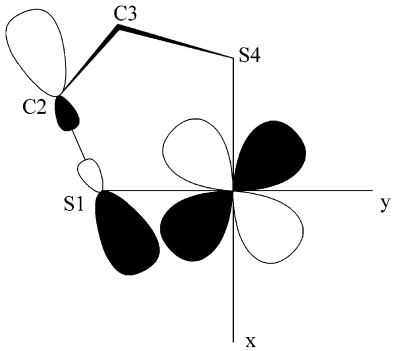

Figure 3. Schematic representation of the spatial overlap between in-plane C−S σ*- and metal t_{2g}-orbitals. C3 lies out of the plane defined by S1, C2, S4, reducing the overlap between C3−S4 σ*- and the d_{xy}-orbital. As a consequence, upon coordination, each thioether group has two inequivalent C−S bond lengths.[5,6]

are slightly larger for the product compound. We find errors of $\Delta d \leq 0.09$ Å (4% of relative error) for the BP functional and of $\Delta d \leq 0.14$ Å (6% of relative error) for BLYP. The largest deviation is observed for one of the rhenium−sulfur bonds (Re−S(3) in Figure 2). For this bond we also observe a relatively large variation of $\Delta d \sim 0.05$ Å upon changing the exchange-correlation functional. These differences indicate that the product state is more sensitive to correlation effects.

The overall agreement for both structures is, however, very satisfying. In particular, the subtle difference in the two C−S bonds of each thioether group ($\langle d1 \rangle = 1.84$ Å and $\langle d2 \rangle = 1.81$ Å in $[Re(9S3)_2]^{2+}$) is reproduced faithfully. In fact, the calculated C−S bonds of the oxidized reactant complex differ by $\Delta d = 0.02$ Å. As suggested previously, the inequivalence of these two bonds is consistent with a possible π-back-donation from donor t_{2g}-orbitals of Re to C−S σ* antibonding ligand orbitals.[5,6] As shown schematically in Figure 3, the thioether group is not planar and upon coordination, only one C−S bond is lying in plane with the filled metal orbitals. The antibonding σ*-orbital of the in-plane C−S bond overlaps more effectively with the metal orbital, resulting in a more efficient back-donation and consequently in a larger C−S bond distance.

The next issue we addressed was the question whether in the observed reductive cleavage reaction the electron transfer and the bond dissociation process occur as simultaneous or consecutive reaction steps. For this purpose, we have determined the effect of the oxidation state of the central metal (i.e., $m = 1,2$) for both undissociated $[Re(9S3)_2]^{m+}$ and dissociated $[Re(9S3)L]^{m+}$ forms of the complex. Since no experimental structural data is available for $[Re(9S3)_2]^{+}$ and $[Re(9S3)L]^{2+}$, we generated these new structures by subtracting and adding one electron to the electronic configurations of the optimized geometries of $[Re(9S3)_2]^{2+}$ and $[Re(9S3)L]^{+}$ and determined the resulting equilibrium structures. Remarkably, our calculations show that the reduced form of the initial complex ($[Re(9S3)_2]^{+}$) corresponds to a stable minimum configuration. This implies that the electron transfer and the bond dissociation process do not take place simultaneously but occur as consecutive reaction steps. The characteristic structural parameters of the reduced and the oxidized form of reactants and products ($[Re(9S3)_2]^{m+}$ and $[Re(9S3)L]^{m+}$, $m = 1$ and 2) are included in Tables 1 and 2, respectively. The calculated bond orders[22] (BOs) (presented in Table 3) parallel the trends in the structural parameters. Surprisingly, the slight differences between the two inequivalent C−S bonds already present in the reactant and product compounds ($[Re(9S3)_2]^{2+}$ and $[Re(9S3)L]^{+}$) is essentially unaffected by a change in oxidation state. Furthermore, despite the observed strong reductive induction of C−S bond breakage, the C−S bond lengths in the oxidized and in the reduced form differ only by a relatively tiny amount ($\Delta d \leq 0.03$ Å; $\Delta BO = 0.03$). This suggests that in the reduced equilibrium structure $[Re(9S3)_2]^{+}$ the strength of the C−S bonds is almost identical to the one in the oxidized form and that the observed reductive induction of C−S bond cleavage is mainly due to a kinetic effect. The slight bond elongation effect upon reduction can be rationalized in terms of a possible π-back-donation. The strength of the C−S bonds is expected to decrease when electron density is transferred from a filled t_{2g}-metal-orbital to a C−S σ*-orbital and an inverse argument can be invoked to rationalize the simultaneous small decrease in Re−S bond lengths. Similar trends upon a change in the oxidation state are also observed in the dissociated products. Consistent with the lowering of symmetry due to the dissociation of one molecule of ethene, the product compounds present two shorter Re−S bonds ($\Delta d < 0.3$ Å; $\Delta BO = 0.05$) at the positions where cleavage of the two C−S bonds has occurred.

TABLE 4: Adiabatic Electron Affinities (EA) Obtained with the BLYP and BP Functionals for the Reactant and Product Compounds (kcal/mol)

	EA	
compound	BLYP	BP
reactant	−198.5	−204.3
product	−216.6	−222.5

To identify specific electronic differences induced by a change in oxidation state, we have performed an analysis of the electronic structure for reactant and product compounds in both charge states. Consistent with the only minor variations in the structural characteristics, the overall electronic structure, as analyzed through a visual inspection of the Kohn−Sham orbitals, turns out to be relatively insensitive to changes in oxidation state. The characteristic nature of the chemically relevant orbitals remains essentially unchanged.

In Table 4, we report the relative energies of reactant and product compounds in the two different oxidation states as given by the corresponding values of the adiabatic electron affinities (EAs). Both functionals result in the same energy ordering. The

TABLE 5: Dissociation Energies and Reaction Energies Barriers (kcal/mol) for the Cleavage of Two C−S Bonds in $[Re(9S3)_2]^{2+}$ and $[Re(9S3)_2]^{+}$ Calculated with BLYP and BP Functionals[a]

	ΔE		E_a	
compound	BLYP	BP	BLYP	BP
$[M(9S3)_2]^{2+}$	14.0	22.1	16.2	20.5
$[M(9S3)_2]^{+}$	4.2	3.7	7.7	9.9

[α] ΔE is the dissociation energy, whereas E_a is the activation energy of the forward reaction.

reduced state is more stable than the oxidized one demonstrating that electron attachment is strongly exothermic ($\Delta E \sim 200$ kcal/mol) for these compounds. However, a significant difference in the reductive stabilization of reactant and product forms can be observed. In fact, both exchange-correlation functionals predict that the product state is more stabilized upon reduction than the reactant complex by ∼18 kcal/mol. In Table 5, the reaction energies for ethene dissociation are reported. These energies, obtained by the relation $\Delta E_{diss} = E_{(product)} + E_{(C_2H_4)} - E_{(reactant)}$, are almost thermoneutral for the reduced form ($\Delta E \sim 4$ kcal/mol) and slightly more endothermic for the oxidized form ($\Delta E \sim 22$ kcal/mol).[23] The BLYP functional predicts somewhat smaller reaction energies, but the same relative trends.

3.2. Molecular Dynamics at Elevated Temperatures. Our calculations of the ground-state properties demonstrate convincingly that the addition/removal of an electron has surprisingly little effect on the overall properties. This seems to be in vast contrast to the experimental observation that the reactive characteristics of these complexes experience a pronounced change in redox active environments. A possible explanation for this apparent contradiction lies in the possibility that the observed differences between oxidized and reduced forms are mainly due to strong variations in their kinetic properties at finite temperature. We therefore proceeded with a thorough investigation of the dynamic behavior of these systems. To this end, we performed first-principles molecular dynamics (Car-Parrinello) simulations at different temperatures for both, the oxidized $[Re(9S3)_2]^{2+}$ and the reduced $[Re(9S3)_2]^{+}$ complexes.[24] In contrast to the pronounced similarity of the equilibrium properties at 0 K, the finite temperature features of oxidized and reduced reactants turn out to be distinctly different.

We performed a first series of MD runs at an average temperature of 300 K. These simulations show that large fluctuations of the C−S bonds ($\langle d \rangle = 1.84$ Å (1.83 ± 0.05 Å and 1.86 ± 0.05 Å, respectively, for the two inequivalent C−S bonds)) are taking place (Figure 4a). These oscillations are slightly more enhanced ($\langle d \rangle = 1.92$ Å (1.90 ± 0.07 Å, 1.94 ± 0.07 Å, respectively) for the reduced form $[Re(9S3)_2]^{+}$ (Figure 4b). For the latter, several C−S bonds show fluctuations up to 2.25 Å. This corresponds to an elongation of 0.35 Å (18%) with respect to the average bond length of 1.90 Å and thus these bonds can be considered as broken. Several of such reactive bond dissociation events can be observed during the 7 ps dynamics runs but they all correspond to processes in which only one of the two C−S bonds of a thioether ligand is broken. Due to the fact that the other C−S bond remains intact, the departing ligand is immediately pulled back within a few femtoseconds. Clearly, for the ethene dissociation to occur, both of the two bonds of a thioether ligand have to be broken. Neither for the oxidized nor for the reduced form of the complex could such a combined event be observed during the limited time (5−7 ps) of our molecular dynamics runs at 300 K. To increase the probability for the occurrence of reactive events, we performed another series of molecular dynamics simulations at a slightly

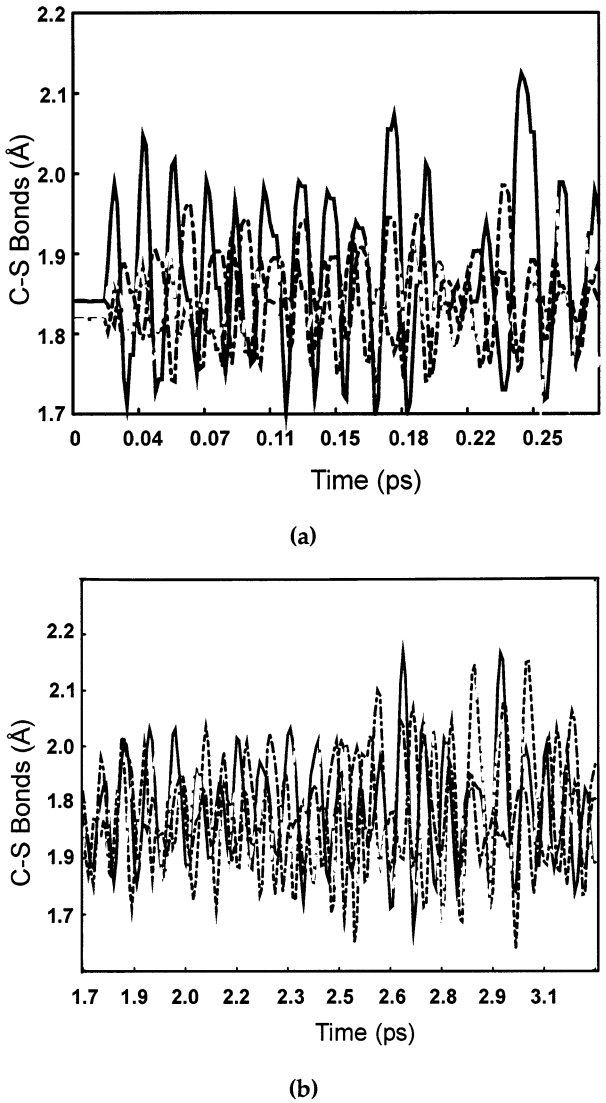

Figure 4. Characteristic C−S bond lengths as a function of simulation time for part of the MD runs performed at 300 K (a) for the oxidized and (b) for the reduced reactant.

enhanced average temperature of 350 K. For the oxidized form of the complex $[Re(9S3)_2]^{2+}$, the increase in temperature merely leads to a slight augmentation in the observed bond fluctuations ($\langle d \rangle = 1.89$ (1.88 ± 0.07 Å, and 1.91 ± 0.07 Å, respectively). For the reduced form $[Re(9S3)L]^{+}$ on the other hand, a spontaneous cleavage reaction with concomitant release of ethene can be observed. A plot of the instantaneous values of the C−S distances during the molecular dynamics trajectory (Figure 5) shows that the breaking of the two critical C−S bonds occurs almost simultaneously. The dissociation event is depicted in a series of representative snapshots in Figure 6. The first frame shows the configuration that the molecule adapts just before the dissociation, after approximately 0.1 ps of simulation time. The simultaneous dissociation of the two C−S bonds occurs after ca. 0.2 ps (frame 2). The third frame (0.3 ps) shows the progressive removal of ethene accompanied by a shortening of the Re−S bonds. In the fourth frame (0.5 ps), the final product is depicted.[25]

For a quantitative determination of the involved dissociation barrier we have followed the system along the observed reaction pathway, performing molecular dynamics runs with constraints along a suitably chosen reaction coordinate. To probe the dependence of the determined activation barriers on the choice

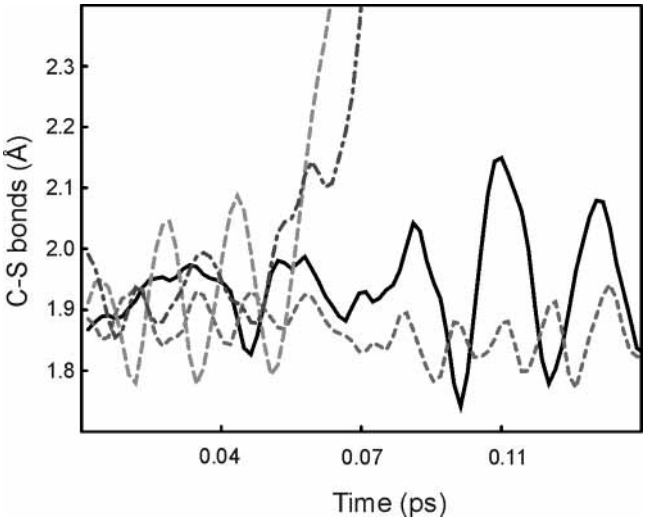

Figure 5. Characteristic C−S bond lengths of $[Re(9S3)_2]^+$ as a function of simulation time for part of the MD runs performed at 350 K.

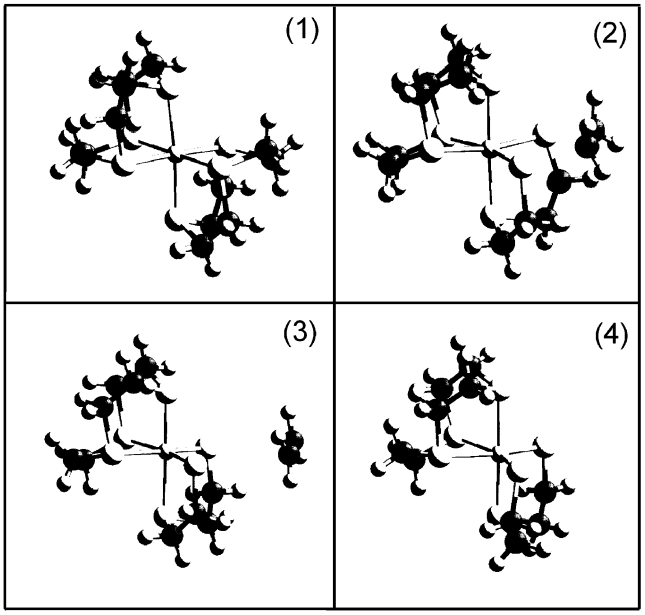

Figure 6. Dissociation pathway of $[Re(9S3)_2]^+$ at 350 K. Snapshots of the most representative frames 1−4 are shown. (1) Conformation of the molecule after 0.1 ps simulation time. (2) Simultaneous dissociation of the two C−S bonds and release of ethene (0.2 ps). (3) Progressive removal of ethene. (4) Formation of the final product.[25]

of constraint, we have performed independent calculations for two different alternative options of the reaction coordinate. In the first case, a dummy atom (D) was placed at the bond midpoint of the two departing carbon atoms (C(16)−C(17)) and a Re−D distance constraint was applied and varied in increments of 0.1 Å. In the second case, a simple bond constraint for one of the two C−S bonds (S(7)−C(17)) of a thioether ligand was chosen and successively augmented in similar intervals. The determination of the transition state for ethene dissociation turned out to be rather difficult as a strong hysteresis effect was observed in particular for the oxidized form. Points close to the maximum of the barrier were therefore determined twice, starting from both reactant and product side. After careful removal of the hysteresis, both choices of reaction coordinates result in identical barrier heights within 0.2 kcal/mol. The final transition states were localized by the change of sign of the average constraint force. Consistent with the experimental observations, the resulting activation energies are substantially

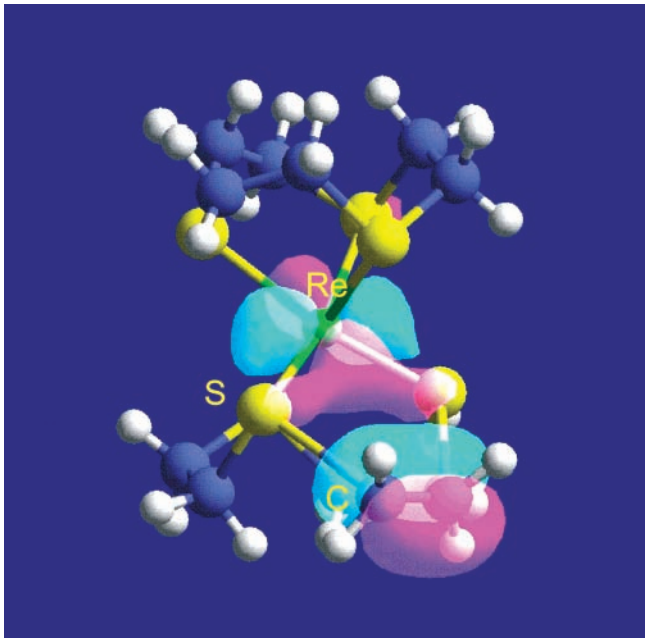

Figure 7. Contour plot of the HOMO-2 orbital at the transition state for $[Re(9S3)_2]^{2+}$ indicating the presence of π-back-donation from one of the d (t_{2g})- orbitals into C−S σ*-ligand orbitals. The contours are given at ±4.0 au.

higher for the oxidized form (Table 5). An activation energy of ∼20.5 (BP) kcal/mol[23] is required for $[Re(9S3)_2]^{2+}$, whereas the dissociation occurs with a barrier of only ∼10 (BP) kcal/mol in the reduced compound $[Re(9S3)_2]^+$. The lower activation energy barrier of the reduced form clearly confirms the importance of the additional electron in promoting the C−S bond cleavage. Calculations based on the BLYP functional predict somewhat smaller values, but the same relative trend.

We note that the dissociation of the two C−S bonds is an entropically favored process. As a consequence, the values of the activation free energies can be expected to be smaller than the calculated activation energies. This is also demonstrated by the fact that we were able to observe the dissociation of a molecule of ethene from the reduced complex at a temperature as low as 350 K during our ∼0.8 ps of first-principles simulations.

An analysis of the bond orders of the transition state structures gives a direct indication of the structural and electronic modifications that take place along the reaction pathway. Consistent with the bonding model involving π-back-donation from rhenium d-orbitals into antibonding C−S σ*-ligand orbitals, the metal−sulfur bonds directly involved in the C−S cleavage reaction (Re−S(6) and Re−S(7)) show enhanced bonding in the transition state. We calculate bond orders of 0.41 and 0.44 in the ground-state structure of $[Re(9S3)_2]^{2+}$ and $[Re(9S3)_2]^+$, respectively, and of 0.77 and 0.82, at the corresponding transition states (Table 3). On the other hand, the bond orders of the two dissociating carbon−sulfur bonds (S(6)−C(16) and S(7)−C(17)) change from values of 0.85 and 0.88 in the ground-state structures of the oxidized and reduced reactant, respectively, to 0.22 and 0.04 at the corresponding transition states. The π-back-donation is further confirmed by a close inspection of the Kohn−Sham orbitals of the transition states as demonstrated with the one-electron orbital (HOMO-2) depicted in Figure 7. In this molecular orbital, one of the t_{2g}-orbitals of the rhenium overlaps with a σ-orbital of the sulfur atom. The symmetry and the phase of the wave function identify this orbital as C−S σ*-orbital. The HOMO-2 of the reduced transition state

structure presents similar features. However, a careful inspection of the bond orders of the transition state structures indicates that the π-back-donation is stronger for the reduced complex. In fact, the dissociating C−S bonds (S(6)−C(16), S(7)−C(17)) are weaker ($\Delta BO = 0.19$) in the transition state of $[Re(9S3)_2]^+$ with respect to the one of $[Re(9S3)_2]^{2+}$, whereas the corresponding Re−S bonds are stronger ($\Delta BO = 0.05$). Furthermore, the C−C bond order of the dissociating ethene (C(16)−C(17)) is essentially the one of the free molecule ($BO \sim 2$) in the transition state structure of the reduced form while it is smaller in the oxidized compound ($BO = 1.6$).

4. Summary and Conclusions

In this article, we present first-principles molecular dynamics studies of the reductive C−S bond cleavage in rhenium hexathioether compounds with stoichiometry $[Re(9S3)_2]^{m+}$ (9S3 = 1,4,7 trithiacyclononane, $m = 1, 2$). The structural, energetic, and electronic properties of reactant and product compounds in the oxidized and reduced states are characterized. Density functional calculations at the gradient-corrected level show that also the reduced form $[Re(9S3)_2]^+$ corresponds to a stable minimum configuration and that the electron transfer and bond dissociation processes take place as consecutive reaction steps. Whereas the additional electron does not have significant effects on the ground-state properties, the structural, electronic, and dynamic features in the transition state are crucially dependent on the oxidation state. Consistent with the experimentally observed reactivity properties, the oxidized form $[Re(9S3)_2]^{2+}$ is stable within picosecond molecular dynamics runs at 300 and 350 K. This is in contrast to the reduced complex $[Re(9S3)_2]^+$ for which we were able to observe a spontaneous cleavage of two C−S bonds and subsequent release of a molecule of ethene. The pronounced change in reactivity upon reduction is reconfirmed by a quantitative determination of the dissociation barriers for which values of ∼21 kcal/mol and ∼10 kcal/mol are obtained for the oxidized and the reduced form, respectively. The significantly lower activation barrier in the reduced form is in agreement with the experimentally observed instability of the rhenium hexathioether compounds toward dissociation in the presence of reducing agents.[5,6]

The observed reactivity pattern can be rationalized by an analysis of the electronic structure in the transition state that indicates a Kohn−Sham orbital (HOMO-2) that is representative for a π-back-donation from a filled metal-orbital into a ligand C−S σ*-orbital with antibonding character. For the reduced compound, the larger electron density at the metal center leads to an enhanced π-back-donation in the transition state and thus to a significant lowering of the barrier for C−S bond cleavage.

Thus, the present study shows that rhenium might serve as highly active promotor in catalysis of HDS reactions.

Acknowledgment. We thank P. J. Blower and G. E. D. Mullen for having suggested this study and for useful discussions.

Supporting Information Available: Test calculations performed on ReF_6 and by the calculation of the ionization potentials of rhenium atom (two tables). This material is available free of charge via the Internet at http://pubs.acs.org.

References and Notes

(1) Dilworth, J. R.; Parrott, S. J. *Chem. Soc. Rev.* **1998**, *27*, 43.
(2) Volkert, W. A.; Jurisson, S. *Technetium Rhenium* **1996**, *176*, 123.
(3) Prakash, S.; Went, M. J.; Blower, P. J. *Nucl. Med. Biol.* **1996**, *23*, 543.
(4) Schoeneich, G.; Palmedo, H.; Heimbach, D.; Biersack, H. J.; Muller, S. C. *Onkologie* **1997**, *20*, 316.
(5) (a) Mullen, G. E. D.; Went, M. J.; Wocadlo, S.; Powell, A. K.; Blower, P. J.; *Angew. Chem., Int. Ed. Engl.* **1997**, *36*, 1205. (b) Mullen, G. E. D.; Blower, P. J.; Price, D. J.; Powell, A. K.; Howard, M. J.; Went, M. J. *Inorg. Chem.* **2000**, *39*, 4093.
(6) Mullen, G. E. D.; Fässler, F. T.; Went, M. J.; Howland, K.; Stein, B.; Blower, P. J. *J. Chem. Soc., Dalton Trans.* **1999**, *21*, 3759.
(7) (a) Gates, B. C.; Katzer, J. R.; Schuit, G. C. A. *Chemistry of Catalytic Processes*; McGraw-Hill: New York, 1979. (b) Prins, R.; de Beer, V. H.; Somorjai, G. A. *Catal. Rev. Sci. Eng.* **1989**, *31*, 1.
(8) (a) Li, J.; Miguel, D.; Morales, M. D.; Riera, V. *Organometallics* **1998**, *17*, 3448. (b) Zhang, X.; Dullaghan, C. A.; Watson, E. J.; Carpenter, G. B.; Sweigart, D. A. *Organometallics* **1998**, *17*, 2067. (c) Dullaghan, C. A.; Carpenter, G. B.; Sweigart D. A.; Choi, D. S.; Lee, S. S.; Chung, Y. K. *Organometallics* **1997**, *16*, 5688. (d) Spera, M. L.; Harman, W. D. *J. Am. Chem. Soc.* **1997**, *119*, 8843 (e) Rakowski Dubois, M. *Chem. Rev.* **1989**, *89*, 1. (f) Feng, Q.; Rauchfuss, T. B.; Wilson, S. R. *Organometallics* **1995**, *14*, 2923. (g) Bianchini, C.; Masi, D.; Meli, A.; Peruzzini, M. Vizza, F.; Zanibini, F. *Organometallics* **1998**, *17*, 2495.
(9) Car, R.; Parrinello, M. *Phys. Rev. Lett.* **1985**, *55*, 2471−2473.
(10) (a) Car, R.; Parrinello, M. Proceedings of NATO ARW: *Simple Molecular System at very High Density*, Les Houches; France; NATO ASI Series; Plenum Press: New York, 1988. (b) Galli, G.; Parrinello, M. In *Computer Simulation in Material Science*; Meyer, M., Pontikis, V., Eds.; Kluwer: Dordrecht, The Netherlands, 1991; p 238 and references therein. (c) Payne, M. C.; Teter, M. P.; Allan, D. C.; Arias, T. A.; Joannoppoulos, J. D. *Rev. Mod. Phys.* **1992**, *64*, 1045. (d) Remler, D. K.; Madden, P. A. *Mol. Phys.* **1990**, *70*, 691. (e) Marx, D.; Hutter, J. *Modern Methods and Algorithms of Quantum Chemistry*; Grotendorst, J., Ed.; Forschungszentrum Juelich, NIC Series, 2000; Vol.1, p 301.
(11) Hutter, J.; Ballone, P.; Bernasconi, M.; Focher, P.; Fois, E.; Goedecker, S.; Parrinello, M.; Tuckerman, M. CPMD; Max-Planck-Institut fuer Festkörperforschung, Stuttgart, and IBM Research Laboratory Zürich, 1998.
(12) Trouiller, M.; Martins, J. L. *Phys. Rev. B* **1991**, *43*, 1993.
(13) Kleinmann, L.; Bylander, D. M. *Phys. Rev. Lett.* **1982**, *48*, 1425.
(14) Becke, A. D. *Phys. Rev. A* **1988**, *38*, 3098.
(15) Perdew, J. P. *Phys. Rev. B* **1986**, *33*, 8822.
(16) Lee, C.; Yang, W.; Parr, R. G. *Phys. Rev. B* **1988**, *37*, 785.
(17) (a) Hockney, R. W. *Methods Compt. Phys.* **1970**, *9*, 136. (b) Barnett, R. N.; Landmann, U. *Phys. Rev. B* **1993**, *48*, 2081.
(18) Matondo, S. O. C.; Moundford, P.; Watkin, D. J.; Jones, W. B.; Cooper, S. R. *J. Chem. Soc., Chem. Commun.* **1995**, 161.
(19) Although, the gas-phase geometry neglects environment effects, the structural trend reproduced by our calculations agrees with the electrospray mass spectroscopy experiments (ref 6).
(20) Ziegler, T. *Density Functional Methods and Material Science*, Wiley: New York, 1997; p 69.
(21) Magistrato, A.; VandeVondele, J.; Rothlisberger, U. *Inorg. Chem.* **2000**, *39*, 5553.
(22) The bond orders reported in the Table 3 are calculated with the BLYP functional on structures that have been optimized at the same level. Calculations of the bond orders have been done according to the scheme proposed by Mayer, I. *Chem. Phys. Lett.* **1983**, *97*, 270. To this end, the plane wave representation of the total wave functions was projected onto an atom-centered minimal basis of atomic pseudo wave functions. This allows a comparison of the bond orders at a qualitative level.
(23) For the oxidized pathway the dissociation limit calculated with the BP functional (22.1 kcal/mol) is 1.6 kcal/mol above the transition state (20.5 kcal/mol). Following the reaction pathway and analyzing the average constraint force we identified a very shallow minimum after the transition state in which the ethene is still weakly coordinated to the central metal. This minimum is stabilized by only 1.2 kcal/mol with respect to a barrier recrossing back to the reactants.
(24) Increasing the temperature of the system allows for an enhanced sampling of the potential energy surface, which makes it possible to follow reaction pathways within the limited time of our simulations (typically of the order of a few tens of picoseconds).
(25) In the fourth frame we do not show the ethene molecule that is still present in the simulation cell.